

Structural phase transition, precursory electronic anomaly, and strong-coupling superconductivity in quasi-skutterudite $(Sr_{1-x}Ca_x)_3Ir_4Sn_{13}$ and $Ca_3Rh_4Sn_{13}$

Jun Luo(罗军), Jie Yang(杨杰), S Maeda, Zheng Li(李政), Guo-Qing Zheng(郑国庆)

Citation: Chin. Phys. B . 2018, 27(7): 077407. **doi:** 10.1088/1674-1056/27/7/077401

Journal homepage: http://cpb.iphy.ac.cn; http://iopscience.iop.org/cpb

What follows is a list of articles you may be interested in

Theory of specific heat of vortex liquid of high T_c superconductors

Chen Bai(白晨), Cheng Chi(迟诚), Jiangfan Wang(王江帆)

Chin. Phys. B . 2016, 25(10): 107404. **doi:** 10.1088/1674-1056/25/10/107404

Parallel variable-density spiral imaging using nonlocal total variation reconstruction

Fang Sheng, Guo Hua

Chin. Phys. B . 2014, 23(5): 057401. **doi:** 10.1088/1674-1056/23/5/057401

Review of nuclear magnetic resonance studies on iron-based superconductors

Ma Long, Yu Wei-Qiang

Chin. Phys. B . 2013, 22(8): 087414. **doi:** 10.1088/1674-1056/22/8/087414

Quenched Fe moment in the collapsed tetragonal phase of $Ca_{1-x}Pr_xFe_2As_2$

Ma Long, Gi Gao-Feng, Dai Jia, Saha S R, Drye T, Paglione J, Yu Wei-Qiang

Chin. Phys. B . 2013, 22(5): 057401. **doi:** 10.1088/1674-1056/22/5/057401

Study on signal intensity of low field nuclear magnetic resonance via indirect coupling measurement

Jiang Feng-Ying, Wang Ning, Jin Yi-Rong, Deng Hui, Tian Ye, Lang Pei-Lin, Li Jie, Chen Ying-Fei, Zheng Dong-Ning

Chin. Phys. B . 2013, 22(4): 047401. **doi:** 10.1088/1674-1056/22/4/047401

RAPID COMMUNICATION

Structural phase transition, precursory electronic anomaly, and strong-coupling superconductivity in quasi-skutterudite $(Sr_{1-x}Ca_x)_3Ir_4Sn_{13}$ and $Ca_3Rh_4Sn_{13}$*

Jun Luo(罗军)[1,2], Jie Yang(杨杰)[1,†], S Maeda[3], Zheng Li(李政)[1,2], and Guo-Qing Zheng(郑国庆)[1,2,3,‡]

[1] *Institute of Physics, Chinese Academy of Sciences, and Beijing National Laboratory for Condensed Matter Physics, Beijing* 100190, *China*
[2] *School of Physical Sciences, University of Chinese Academy of Sciences, Beijing* 100049, *China*
[3] *Department of Physics, Okayama University, Okayama* 700-8530, *Japan*

(Received 9 April 2018; revised manuscript received 2 May 2018; published online 25 June 2018)

The interplay between superconductivity and structural phase transition has attracted enormous interest in recent years. For example, in Fe-pnictide high temperature superconductors, quantum fluctuations in association with structural phase transition have been proposed to lead to many novel physical properties and even the superconductivity itself. Here we report a finding that the quasi-skutterudite superconductors $(Sr_{1-x}Ca_x)_3Ir_4Sn_{13}$ ($x = 0$, 0.5, 1) and $Ca_3Rh_4Sn_{13}$ show some unusual properties similar to the Fe-pnictides, through ^{119}Sn nuclear magnetic resonance (NMR) measurements. In $(Sr_{1-x}Ca_x)_3Ir_4Sn_{13}$, the NMR linewidth increases below a temperature T^* that is higher than the structural phase transition temperature T_s. The spin-lattice relaxation rate $(1/T_1)$ divided by temperature (T), $1/T_1T$ and the Knight shift K increase with decreasing T down to T^*, but start to decrease below T^*, and followed by more distinct changes at T_s. In contrast, none of the anomalies is observed in $Ca_3Rh_4Sn_{13}$ that does not undergo a structural phase transition. The precursory phenomenon above the structural phase transition resembles that occurring in Fe-pnictides. In the superconducting state of $Ca_3Ir_4Sn_{13}$, $1/T_1$ decays as $\exp(-\Delta/k_BT)$ with a large gap $\Delta = 2.21k_BT_c$, yet without a Hebel–Slichter coherence peak, which indicates strong-coupling superconductivity. Our results provide new insight into the relationship between superconductivity and the electronic-structure change associated with structural phase transition.

Keywords: nuclear magnetic resonance, antiferromagnetic fluctuation, structural phase transition, phase diagram

PACS: 74.25.nj, 74.40.–n, 74.25.Dw **DOI:** 10.1088/1674-1056/27/7/077401

1. Introduction

Transition-metal compounds show diverse properties such as magnetism, superconductivity, and charge density wave, and often accompany a structural transition.[1–3] In these materials, the interplay between superconductivity and other orders is of great interest. For example, in the copper oxides,[4] heavy fermions,[5] and iron-based superconductors[6] that contain transition metal elements, superconductivity is found in the vicinity of a quantum critical point (QCP) at which other orders are completely suppressed at absolute zero temperature. In particular, in iron-based superconductors, not only a magnetic (spin density wave) QCP, but also another QCP associated with the structural phase transition exists.[7] In this case, quantum fluctuations of the electronic nematic order associated with the structural phase transition may lead to many novel physical properties such as T-linear electrical resistivity.[7–10]

Materials with the general stoichiometry $R_3M_4X_{13}$ are a large family usually adopting a common quasi-skutterudite structure, where R is an alkaline-earth or rare-earth element, M is a transition metal, and X is a group-IV element.[11,12] Superconductivity with a fairly high transition temperature $T_c \sim 7$ K was found in $R_3M_4Sn_{13}$ more than 30 years ago,[13,14] but the physical properties were poorly understood. Recently, this class of materials received new attention because of a possible interplay between the superconductivity and the structure instability.

The electrical resistivity, susceptibility, Hall coefficient, and heat transport measurements on $Ca_3Ir_4Sn_{13}$ found that an anomaly occurs at a temperature of 35 K, above the superconducting transition temperature $T_c = 7$ K.[15–17] The anomaly was ascribed to ferromagnetic spin fluctuation in early works.[15] Resistivity and susceptibility measurements on $Sr_3Ir_4Sn_{13}$ also showed anomalies at 147 K. Subsequent x-ray diffraction and pressure effect measurements on $Sr_3Ir_4Sn_{13}$ showed that a structural phase transition from a

*Project supported by the National Natural Science Foundation of China (Grant Nos. 11674377 and 11634015), the National Key R&D Program of China (Grant Nos. 2017YFA0302904 and 2016YFA0300502), and the Strategic Priority Research Program (B) of the Chinese Academy of Sciences (Grant No. XDB07020200). J. Y. is supported by the Youth Innovation Promotion Association of CAS.

†Corresponding author. E-mail: yangjie@iphy.ac.cn
‡Corresponding author. E-mail: gqzheng123@gmail.com

© 2018 Chinese Physical Society and IOP Publishing Ltd

cubic I phase ($Pm\bar{3}n$) to an I′ phase ($I\bar{4}3d$) takes place at T_s, with the lattice parameter doubled in the low temperature phase. Therefore, the anomalies reported earlier in this class of materials are due to the structural phase transition. By chemical or physical pressure, T_s can be suppressed to zero, while T_c increases slowly and reaches to a maximum 8.9 K.[18] A similar phase diagram has also been obtained in $(Sr_{1-x}Ca_x)_3Rh_4Sn_{13}$.[19] Thus, a possible relation between the enhanced T_c and the structure instability was suggested.[18,20]

The nature of the electronic structure change due to the structural phase transition is not well understood. Neutron scattering and specific heat measurements revealed a second-order nature of the structural phase transition in $(Sr_{1-x}Ca_x)_3Ir_4Sn_{13}$.[21,22] The Hall coefficient changed from a negative to a positive value and the optical measurement indicated that the Drude spectral weight is transferred to the high energy region across T_s in $Sr_3Ir_4Sn_{13}$.[23,24] Based on these results, a reconstruction of the Fermi surface below T_s due to a charge density wave (CDW) formation was suggested.[23,24]

In this work, we grow single crystals of $(Sr_{1-x}Ca_x)_3Ir_4Sn_{13}$ ($x = 0$, 0.5, 1) and $Ca_3Rh_4Sn_{13}$, and perform electrical resistivity and ^{119}Sn NMR measurements to elucidate the electronic properties change associated with the structural phase transition. $(Sr_{1-x}Ca_x)_3Ir_4Sn_{13}$ ($x = 0$, 0.5, 1) undergo a structural phase transition at $T_s = 147$ K, 85 K, and 35 K, respectively, while $Ca_3Rh_4Sn_{13}$ does not. By NMR measurements, we find that an anomaly occurs already above T_s in $(Sr_{1-x}Ca_x)_3Ir_4Sn_{13}$ ($x = 0$, 0.5, 1). Such an electronic anomaly prior to the structural transition resembles an actively-investigated phenomenon in some of the Fe-based superconductors where the physical properties show an in-plane anisotropy (nematicity) above T_s below which the C_4 symmetry is lowered to the C_2 symmetry. However, in $Ca_3Rh_4Sn_{13}$ that does not undergo a structural transition, the Korringa relation is satisfied down to $T \sim 20$ K. The electronic state properties below T^* are discussed by analyzing the change in the Korringa ratio. We also measure the superconducting state property of $Ca_3Ir_4Sn_{13}$, and find that it is a strong-coupling s-wave superconductor. We will discuss the relationship between the superconductivity, the electronic state change associated with the structural transition, and electron correlations.

2. Experiment

Single crystals of $(Sr_{1-x}Ca_x)_3Ir_4Sn_{13}$ and $Ca_3Rh_4Sn_{13}$ were grown by the self-flux method, as previously reported in Ref. [13]. The composition shown in this paper is the nominal one. Excessive Sn flux was removed in concentrated HCl acid. Crystals with the proper size were picked up and polished, then the temperature dependence of the resistivity was measured by the standard four-probe method using a physical properties measurement system (PPMS, Quantum Design). The T_c was determined by both DC susceptibility using a magnetic properties measurement system (MPMS, Quantum Design) with an applied magnetic field of 10 Oe, and AC susceptibility using an *in-situ* NMR coil. For ^{119}Sn NMR measurements, since the sample shows a good electrical conductivity so that the skin depth is short, we crushed the single crystals into fine powders to gain the surface area. The ^{119}Sn nucleus has a nuclear spin $I = 1/2$ and gyromagnetic ratio $\gamma_n/2\pi = 15.867$ MHz/T. The ^{119}Sn NMR spectra were obtained by scanning the rf frequency and integrating the spin echo intensity at a fixed magnetic field H_0. The spin-lattice relaxation time T_1 was measured by using the saturation-recovery method, and obtained by a good fitting of the nuclear magnetization $M(t)$ to $1 - M(t)/M_0 = \exp(-t/T_1)$, where $M(t)$ is the nuclear magnetization at time t after the single saturation pulse and M_0 is the nuclear magnetization at thermal equilibrium.

3. Results

3.1. Sample characterization

Figure 1(a) presents the temperature dependence of the electrical resistivity for $(Sr_{1-x}Ca_x)_3Ir_4Sn_{13}$ ($x = 0$, 0.5, 1) and $Ca_3Rh_4Sn_{13}$ single crystals. For $(Sr_{1-x}Ca_x)_3Ir_4Sn_{13}$ ($x = 0$, 0.5, 1), the resistivity shows a distinct hump, which has been ascribed to a structure transition.[18] Figure 1(b) shows the

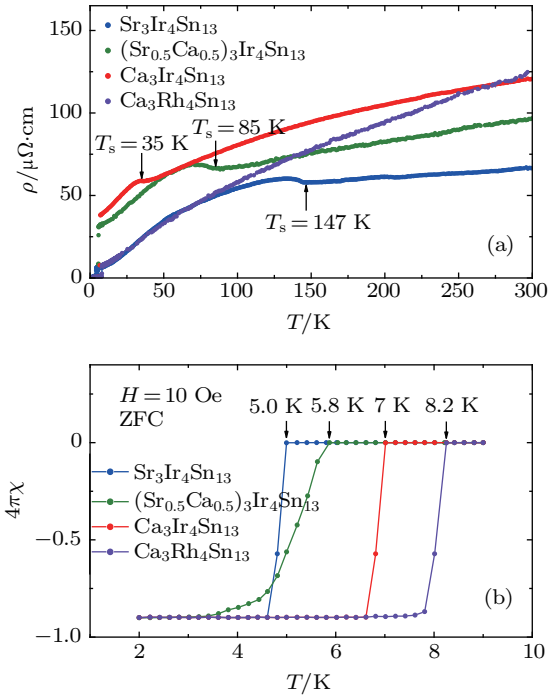


Fig. 1. (color online) (a) The temperature dependence of the electrical resistivity for $(Sr_{1-x}Ca_x)_3Ir_4Sn_{13}$ ($x = 0$, 0.5, 1) and $Ca_3Rh_4Sn_{13}$. The arrows indicate the structural transition temperature T_s. (b) The temperature dependence of the magnetic susceptibility for $(Sr_{1-x}Ca_x)_3Ir_4Sn_{13}$ ($x = 0$, 0.5, 1) and $Ca_3Rh_4Sn_{13}$ below $T = 9$ K. The arrows indicate the critical temperature T_c.

temperature dependence of the DC magnetic susceptibility below 9 K. A sharp superconducting transition with a narrow transition width of about 0.2 K for $Sr_3Ir_4Sn_{13}$, $Ca_3Ir_4Sn_{13}$, and $Ca_3Rh_4Sn_{13}$ indicates the good crystal quality. The T_c is determined by the point at which the magnetic susceptibility begins to decrease. The Meissner shielding fraction is estimated to be over 90%, which proves the bulk nature of the superconductivity.

3.2. Precursory electronic anomaly above T_s

Since ^{119}Sn ($I = 1/2$) has no quadrupole moment, the nuclear spin Hamiltonian is simply given by the Zeeman interaction $\mathcal{H} = -\gamma_n \hbar H_0(1+K)\hat{I}$, where K is the Knight shift and γ_n is the nuclear gyromagnetic ratio. As expected in a material with a cubic crystal structure, a single ^{119}Sn NMR transition line ($m = -1/2 \leftrightarrow m = 1/2$ transition) is observed. Considering that the Sn atoms form an icosahedral cage in the crystal structure and there are two different crystallographic sites (see Fig. 2), namely, one Sn(1) in the center and twelve Sn(2) on the vertices of the icosahedron, the spectrum should have two peaks. Figure 2 shows the frequency-swept ^{119}Sn-NMR spectra measured at $T = 250$ K under a fixed magnetic field for the four samples. It can be seen that the spectra indeed show two peaks. All the spectra can be fitted by two Gaussian functions with an area ratio of 12 : 1, so the low frequency peak and high frequency peak respectively correspond to Sn(2) and Sn(1), which have an occupancy ratio of 12 : 1. The typical fitting curves at 250 K are shown in Fig. 2.

Below we discuss the normal-state properties inferred from the NMR measurements. Figure 3 shows the temperature dependence of the spectra for the four samples, from which the full width at half maximum (FWHM) of the spectra is obtained as shown in Fig. 4. Usually, one expects that the FWHM of the spectra increases below the structural phase transition temperature, below which four types of Sn(2) sites are formed[18] that may have slightly different K and result in broadening of the spectra. However, as can be seen in Fig. 4, the FWHM starts to increase at a temperature T^* that is above T_s.

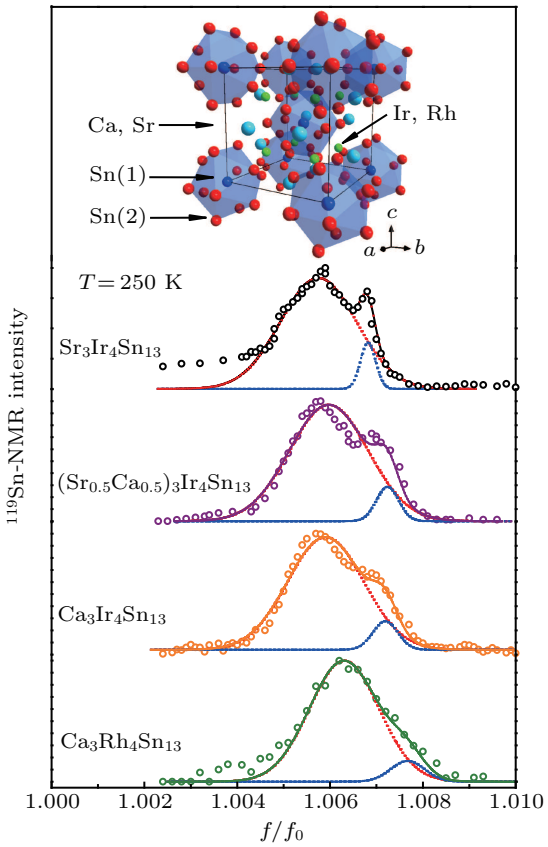


Fig. 2. (color online) The crystal structure of $(Sr_{1-x}Ca_x)_3Ir_4Sn_{13}$ and $Ca_3Rh_4Sn_{13}$ that contain two different Sn sites, and the ^{119}Sn-NMR spectra for $(Sr_{1-x}Ca_x)_3Ir_4Sn_{13}$ ($x = 0, 0.5, 1$) and $Ca_3Rh_4Sn_{13}$ at 250 K. The horizontal coordinate represents the reduced frequency f/f_0, with $f_0 = \gamma H_0/2\pi$. The blue and red dotted lines are Gaussian fittings to the obtained spectra with area ratio of 1 : 12. The solid lines are the sum of the two Gaussian functions.

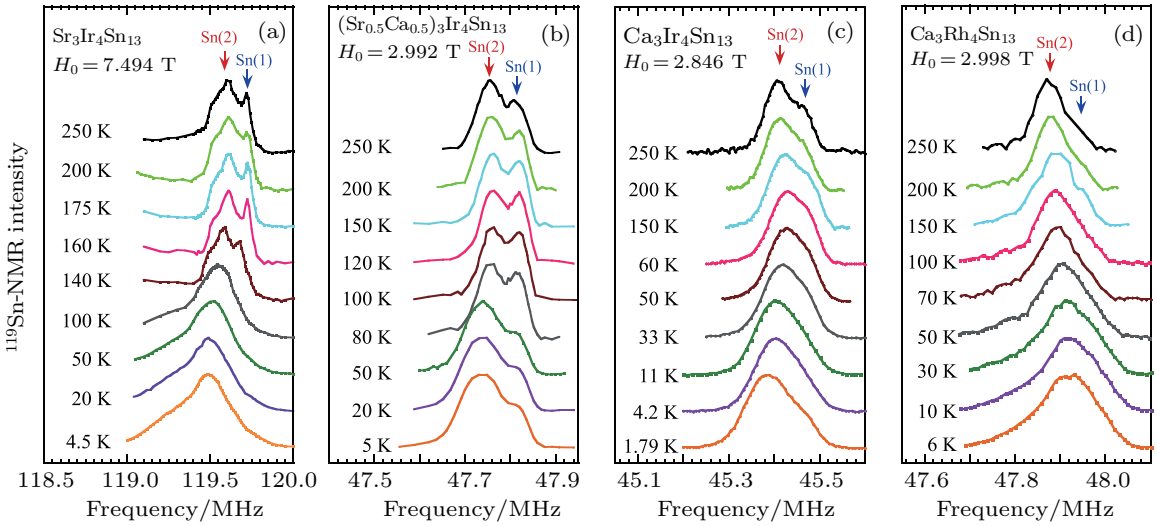


Fig. 3. (color online) The temperature dependence of the ^{119}Sn-NMR spectra for (a)–(c) $(Sr_{1-x}Ca_x)_3Ir_4Sn_{13}$ ($x = 0, 0.5, 1$) and (d) $Ca_3Rh_4Sn_{13}$. The two peaks marked by the blue and red arrows correspond to Sn(1) site and Sn(2) site, respectively.

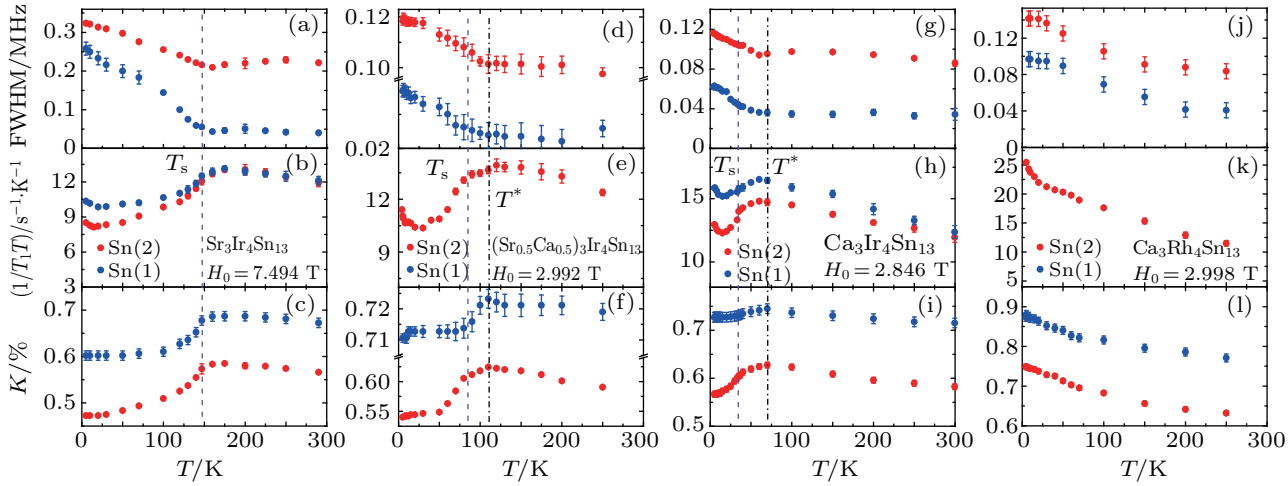


Fig. 4. (color online) The temperature dependence of FWHM of the NMR spectra, $1/T_1T$, and the Knight shift K of (a)–(i) $(Sr_{1-x}Ca_x)_3Ir_4Sn_{13}$ ($x = 0$, 0.5, 1) and (j)–(l) $Ca_3Rh_4Sn_{13}$. The blue and red filled circles correspond to Sn(1) and Sn(2) sites, respectively. The purple dash lines indicate structural transition temperature T_s. The black dash dot lines indicate the temperature T^* below which anomalies appear.

Figure 4 also shows the temperature dependence of $1/T_1T$ and the Knight shift K for the four samples. The K was obtained from the Gaussian fitting of the spectra. T_1 was measured at the position of the respective two peaks. It can be seen that $1/T_1T$ and K also decrease below T^*, and followed by a more distinct change at T_s. For $(Sr_{0.5}Ca_{0.5})_3Ir_4Sn_{13}$ and $Ca_3Ir_4Sn_{13}$, the anomaly is pronounced, although it is less clear for $Sr_3Ir_4Sn_{13}$. A previous report in $Ca_3Ir_4Sn_{13}$ that $1/T_1T$ decreases below around 75 K is consistent with our results.[25]

The total Knight shift consists of three parts, $K = K_{dia} + K_{orb} + K_s$, where K_{dia} arises from the diamagnetic susceptibility χ_{dia}, K_{orb} from the orbital (Van-Vleck) susceptibility χ_{orb}, and K_s from the spin susceptibility χ_s. The χ_s is estimated to be 8.1×10^{-4} emu/mol according to $\chi_s = 2\mu_B^2 N(0)$, where $N(0) = 12.5$ eV^{-1} per formula unit is the density of states at the Fermi level.[26] The closed shells or fully occupied electronic bands contribute to the diamagnetism, which is proportional to the atomic number and the atomic radius. Since iridium has a large atomic number, the reported diamagnetic susceptibility of $Sr_3Ir_4Sn_{13}$, which is -1.2×10^{-4} emu/mol above T_s,[18,23] is mainly due to iridium, whose contribution is -9.8×10^{-4} emu/mol.[15] The χ_{orb} is temperature-independent, and is usually much smaller than χ_s. After considering different contributions, the total susceptibility can be diamagnetic as reported.[18,23] However, the Ir diamagnetism has no hyperfine coupling to Sn nuclear spins. Thus the Sn Knight shift is mainly due to χ_s, and is positive, as found in our measurement.

In general, $1/T_1T$ probes the transverse imaginary part of the dynamic susceptibility $(\chi''_\perp(q,\omega))$ and can be written as

$$\frac{1}{T_1T} = \frac{2\gamma_n{}^2 k_B}{(\gamma_e\hbar)^2} \sum_q |A(q)|^2 \frac{\chi''_\perp(q,\omega)}{\omega}, \qquad (1)$$

where $A(q)$ is the hyperfine coupling constant, ω is the NMR frequency, and γ_e is the electronic gyromagnetic ratio. In a simple metal with no electron correlation, $1/T_1T$ is reduced to a constant proportional to $N(0)^2$. On the other hand, K_s due to spin susceptibility is proportional to $N(0)$. As a result, a relation between the two quantities (Korringa relation), $T_1TK_s^2 = \frac{\hbar}{4\pi k_B}(\frac{\gamma_e}{\gamma_n})^2$, is obtained. Therefore, a decrease of $1/T_1T$ and K below T_s is usually encountered, as a reduction of the density of states (DOS) can be expected. A closer look into the data finds that $1/T_1T$ and K decrease more rapidly at the Sn(2) site than that at the Sn(1) site. This indicates that the Sn(2) site has a closer relationship with the transition. This is consistent with the neutron and x-ray scttering experiments that have found a breathing mode of phonon due to Sn(2) atoms, which is softened at T_s.[21] In contrast to $(Sr_{1-x}Ca_x)_3Ir_4Sn_{13}$ ($x = 0$, 0.5, 1), we did not detect any anomaly in the temperature dependence of $1/T_1T$, K, and FWHM of $Ca_3Rh_4Sn_{13}$ above 20 K, as shown in Fig. 4(j)–4(l). This is consistent with the fact that $Ca_3Rh_4Sn_{13}$ does not undergo a structural phase transition.

The anomaly seen in $1/T_1T$ and K at T^* resembles a puzzling phenomenon in the Fe-based superconductors such as $BaFe_{2-x}Co_xAs_2$, $BaFe_2(As_{1-x}P_x)_2$, or $NaFe_{1-x}Co_xAs$,[27–29] where nematic properties already appear at a temperature far above T_s. In this class of Fe-based materials, a C_4 to C_2 structural phase transition place at T_s. It also shares some similarities with the pseudogap behaviors in underdoped copper oxide superconductors, where the DOS starts to decrease before the superconducting phase transition.[30] In any event, the precursory electronic anomaly above the T_s suggests that the structural phase transition is electronically-driven, rather than lattice-driven.

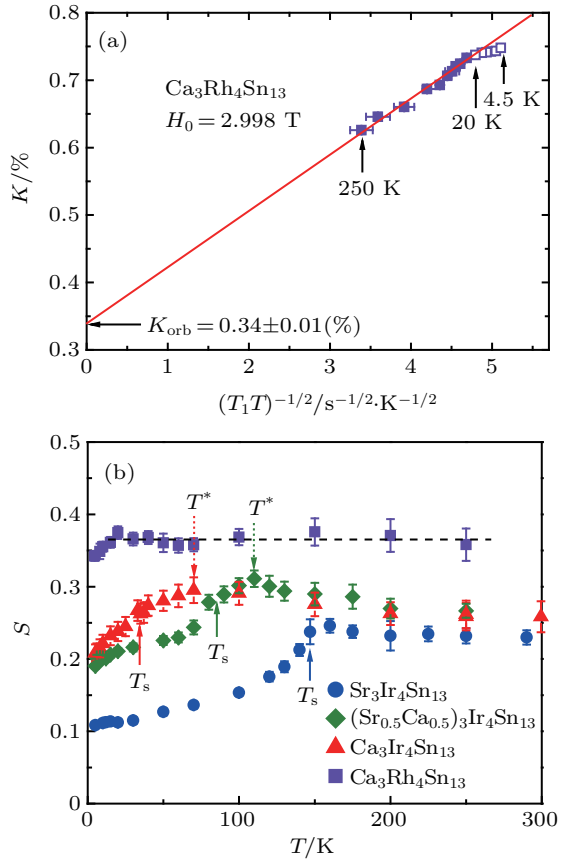


Fig. 5. (color online) (a) The relationship between $(T_1T)^{-1/2}$ and K for $Ca_3Rh_4Sn_{13}$, with temperature as an implicit parameter. The red solid line is a linear fitting to the data above $T = 20$ K. The solid violet squares and open violet squares represent points above and below 20 K, respectively. (b) The Korringa ratio as a function of temperature for $(Sr_{1-x}Ca_x)_3Ir_4Sn_{13}$ ($x = 0$, 0.5, 1) and $Ca_3Rh_4Sn_{13}$. The dash arrows indicate T^*. The solid arrows indicate T_s. The dashed straight line is the guide to the eyes.

3.3. Electronic-state change below T^*

Next, we examine if the electronic-state change below T^* can be totally ascribed to a loss of the DOS. In Fig. 5(a), we plot K against $(T_1T)^{-1/2}$ for $Ca_3Rh_4Sn_{13}$. In the temperature range 20 K$< T <$ 250 K, a good linear relation is found between K and $(T_1T)^{-1/2}$, as expected for a conventional metal in which both $(T_1T)^{-1/2}$ and K_s are proportional to the DOS. Deviation from the linear relation below $T = 20$ K will be discussed later. From the intercept of the relation, we obtain $K_{orb} = 0.34 \pm 0.01\%$.

For $(Sr_{1-x}Ca_x)_3Ir_4Sn_{13}$ ($x = 0$, 0.5, 1), however, the temperature dependence of $(T_1T)^{-1/2}$ and K is weak at high temperatures so that a similar plot does not yield meaningful information. Instead we plot the so-called Korringa ratio S as a function of temperature in Fig. 5(b), where S is defined as

$$S = \frac{4\pi k_B T_1 T K_s^2}{\hbar}\left(\frac{\gamma_n}{\gamma_e}\right)^2. \quad (2)$$

For a conventional metal, $S = 1$. As one can see, S is constant for $Ca_3Rh_4Sn_{13}$ above $T = 20$ K within the experimental error, which is also true for $(Sr_{1-x}Ca_x)_3Ir_4Sn_{13}$ above T^*. However, S shows a distinct decrease below T^* for $(Sr_{1-x}Ca_x)_3Ir_4Sn_{13}$, which suggests that the reduction of $1/T_1T$ and K cannot simply be ascribed to a loss of the DOS. Below, we discuss possibilities for the decrease of S.

Firstly, a second-order phase transition often accompanies the development of a short-range correlation just above the transition temperature, thus the structural instability may be responsible for the anomaly seen in our NMR data. Theoretical calculations of phonon dispersion suggest that imaginary phonon modes exist in $Sr_3Ir_4Sn_{13}$ and the lattice instabilities lie at some wave vectors.[26] Neutron scattering data have shown the softening of phonon mode towards T_s.[21] Specific heat measurements on $Sr_3Ir_4Sn_{13}$ also show that $\Delta C/T$ starts to increase at 160 K ($T_s = 147$ K) and the critical fluctuation model can fit the specific heat data well, which leads to the proposal of short-range correlation above T_s.[22] Therefore, the NMR quantities may also be affected by such structural short-range correlation through magneto–elastic coupling, resulting in the deviation from the Korringa relation below T^*. On the other hand, we note that, for a CDW case, the quantity $1/T_1T$ will increase with decreasing temperature towards the transition temperature,[31,32] in contrast to a decrease of $1/T_1T$ observed in the present case.

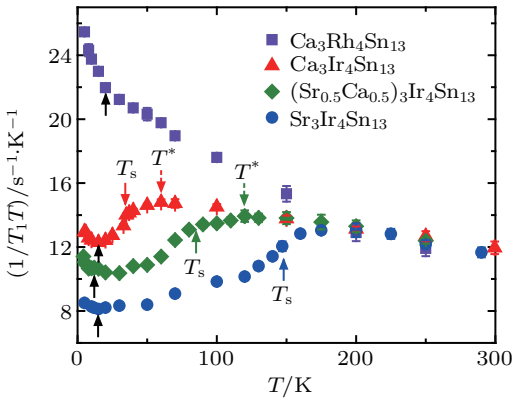


Fig. 6. (color online) The temperature dependence of $1/T_1T$ for $(Sr_{1-x}Ca_x)_3Ir_4Sn_{13}$ ($x = 0$, 0.5, 1) and $Ca_3Rh_4Sn_{13}$. The dash arrows indicate T^*. The solid arrows indicate T_s. The solid black arrows mark the temperature below which $1/T_1T$ shows an upturn.

Secondly, we discuss the possibility of magnetic correlations. To explore this issue in more detail, we turn to the data at temperatures below $T = 20$ K. In Fig. 6, we compare $1/T_1T$ of the four samples. Above 160 K, $1/T_1T$ for all samples has the same value and shows a similar temperature variation. Below 160 K, $1/T_1T$ of $Ca_3Rh_4Sn_{13}$ increases all the way down to 4.2 K, while that of $(Sr_{1-x}Ca_x)_3Ir_4Sn_{13}$ is reduced below T^*. Interestingly, we note that, in all samples, there exists an upturn at a low temperature below $T = 20$ K, as indicated by the black arrows. Such upturn is quite pronounced particularly in $Ca_3Rh_4Sn_{13}$. It can be seen from Fig. 4 that $1/T_1T$ shows a clear upturn for $(Sr_{1-x}Ca_x)_3Ir_4Sn_{13}$, while the Knight shift is T-independent in such a temperature range.

For $Ca_3Rh_4Sn_{13}$, the temperature dependencies of $1/T_1T$ and K also deviate from the Korringa relation below $T = 20$ K due to the additional increase of $1/T_1T$. Therefore, the upturn is clearly not due to a change in the DOS or the structural instability, since the upturn is away from T_s and $Ca_3Rh_4Sn_{13}$ even does not undergo a structural phase transition. Previously, anharmonic phonons due to the rattling motion of the ions inside the cage have been proposed to contribute an additional relaxation,[33] and possibly have been seen in filled-skutterudites $LaOs_4Sb_{12}$ and $LaPt_4Ge_{12}$.[34,35] In the systems, one might also expect that the Sn(1) atoms rattle inside the cage and contribute additionally to $1/T_1T$. However, our data show that the Sn(1) and Sn(2) sites exhibit the same behavior, even though the Sn(2) atoms are not involved in the rattling motion. Therefore, the possibility of rattling as a cause for the upturn in $1/T_1T$ may be excluded. Rather, the rise of $1/T_1T$ at low temperatures likely originates from antiferromagnetic spin fluctuations, which cause an increase of $\chi''_\perp(q,\omega)$ at a finite q when the temperature is lowered. Therefore, coming back to Fig. 5(b), we believe that, the reduction of S is more likely due to antiferromagnetic spin fluctuations that develop below T^* and become more evident at low temperatures.

3.4. Phase diagram

In Fig. 7, we display the phase diagram of $(Sr_{1-x}Ca_x)_3Ir_4Sn_{13}$ ($x = 0$, 0.5, 1) and $Ca_3Rh_4Sn_{13}$. The lattice constant of $(Sr_{1-x}Ca_x)_3Ir_4Sn_{13}$ shrinks linearly upon substituting Sr with Ca. Therefore, increasing calcium content x is equivalent to applying a hydrostatic pressure (P).[18] We note that Hu *et al.* have also scaled $(Sr_{1-x}Ca_x)_3Ir_4Sn_{13}$ and $(Sr_{1-x}Ca_x)_3Rh_4Sn_{13}$ in one phase diagram.[36] When a pressure of 25.7 kbar is applied to $Sr_3Ir_4Sn_{13}$, T_s and T_c become almost the same as those of $(Sr_{0.5}Ca_{0.5})_3Ir_4Sn_{13}$. Such a phenomenon also occurs between $(Sr_{0.5}Ca_{0.5})_3Ir_4Sn_{13}$ and $Ca_3Ir_4Sn_{13}$.[18] These results suggest that the change in x ($\Delta x = 1$) corresponds to a change in pressure of $\Delta P = 52$ kbar. The T_s extrapolates to zero temperature at $P = 18$ kbar in $Ca_3Ir_4Sn_{13}$.[18] In the $(Sr_{1-x}Ca_x)_3Rh_4Sn_{13}$ series, T_s extrapolates to zero temperature at $x = 0.9$, or equivalently, at $P = -6.8$ kbar relative to $Ca_3Rh_4Sn_{13}$.[19] Based on these results, we obtain the relative pressure for our samples with respect to $Ca_3Ir_4Sn_{13}$, and construct a phase diagram as shown in Fig. 7.

As the pressure increases, T_s and T^* are suppressed while T_c increases slowly, which means that there exists a competition between the structural phase transition and superconductivity. A similar phase diagram has been seen in other systems such as $LaPt_{2-x}Ge_{2+x}$,[37] where T_c increases from 0.41 K to 1.95 K and T_s decreases from 394 K to 50 K. Note that the Knight shift and thus the electronic DOS remain T-independent at low temperatures, while its absolute value increases from $Sr_3Ir_4Sn_{13}$ to $Ca_3Rh_4Sn_{13}$. Therefore, the increase of DOS may be partly responsible for the increase of T_c.

$Ca_3Rh_4Sn_{13}$ is located near the end point of the T^* curve, and its superconducting transition temperature $T_c = 8$ K is close to the highest value of this class of materials under chemical or physical pressures. In cuprates and Fe-based superconductors, T_c has a close connection to magnetic fluctuations or structural/orbital fluctuations. Although it is not clear at the moment how the antiferromagnetic spin fluctuations found in this work are related to the structural phase transition, the antiferromagnetic spin fluctuations may also contribute to the increase of T_c. In fact, a systematic change of the Korringa ration S is found as the chemical pressure is increased, as seen in Fig. 5(b). This is a direction to be explored in the future.

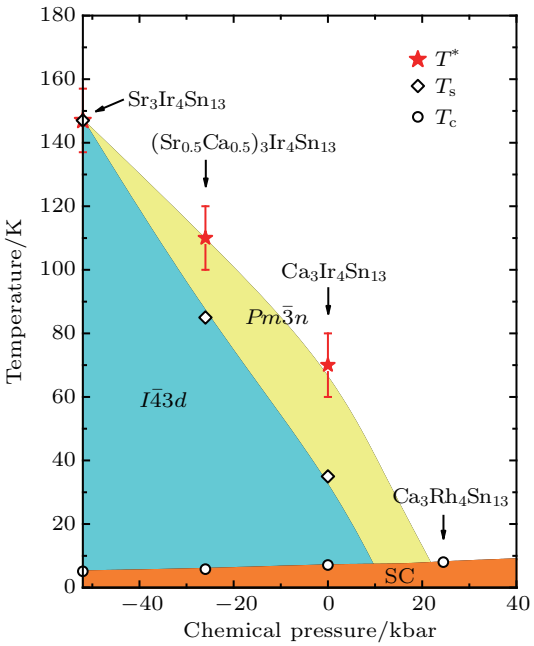


Fig. 7. (color online) The phase diagram of $(Sr_{1-x}Ca_x)_3Ir_4Sn_{13}$ ($x = 0$, 0.5, 1) and $Ca_3Rh_4Sn_{13}$. T^* and T_s are obtained from NMR spectral line width, $1/T_1T$, and the Knight shift. For $Sr_3Ir_4Sn_{13}$, the anomaly above T_s can be identified from $1/T_1T$ but less clear in FWHM and K, thus we plot $T^* = T_s \pm 10$ K. The yellow region is a crossover rather than a new phase. The correspondence between the pressure and the composition is inferred from Refs. [18] and [19].

3.5. Superconducting properties

In this section, we discuss the properties of $Ca_3Ir_4Sn_{13}$ in the superconducting state. In order to minimize the effect of the external field, we have performed NMR measurements for the Sn(2) site under a low field of $H_0 = 0.4$ T that is much smaller than $H_{c2} \approx 7$ T. The T_c is 6.4 K at $H_0 = 0.4$ T. The ^{119}Sn Knight shift below $T_c(H)$ is shown in Fig. 8(a). At the low temperature of 1.5 K, the Knight shift approaches a value of 0.32%, which is very close to $K_{orb} = 0.34 \pm 0.01\%$ obtained from Fig. 5(a) for $Ca_3Rh_4Sn_{13}$. The small excess reduction at $T = 1.5$ K (by about 0.02%) could be due to the diamagnetism of the vortex lattice.[38] The result indicates that the spin susceptibility vanishes completely at $T = 1.5$ K, which indicates

that the Cooper pairs are in the spin-singlet state.

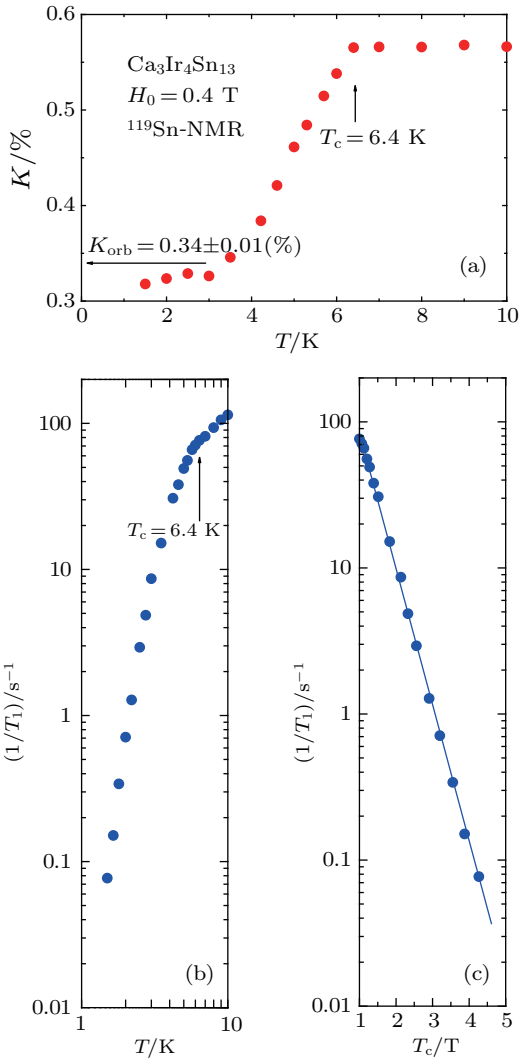


Fig. 8. (color online) (a) The temperature dependence of the Knight shift for $Ca_3Ir_4Sn_{13}$ at $H_0 = 0.4$ T. The arrow indicates T_c. (b) The temperature dependence of $1/T_1$ below 10 K. (c) The temperature dependence of $1/T_1$ below T_c in semilogarithmic coordinate. The solid line represents the relation $1/T_1 \propto \exp(-\Delta/k_BT)$.

Figure 8(b) shows the temperature dependence of $1/T_1$. There are two noticeable features. One is that $1/T_1$ decreases exponentially over three decades with decreasing temperature. The other is that $1/T_1$ shows no Hebel–Slichter coherence peak just below T_c. The lack of a Hebel–Slichter coherence peak was previously reported in filled-skutterudite $PrOs_4Sb_{12}$.[39] To see the decay more intuitively, we replot $1/T_1$ in a semilogarithmic scale in Fig. 8(c). As can be seen, a straight line of the relation $1/T_1 \propto \exp(-\Delta/k_BT)$ fits the data well down to 1.5 K, where Δ and k_B denote the superconducting energy gap at $T = 0$ and the Boltzmann constant, respectively. The fitting parameter $2\Delta = 4.42k_BT_c$ is obtained, which is larger than the BCS gap size $2\Delta = 3.53k_BT_c$. Our result is different from an earlier NMR measurement on $Ca_3Ir_4Sn_{13}$, where a small Hebel–Slichter peak was claimed.[40] The large superconducting energy gap suggests strong-coupling superconductivity, which is consistent with the muon spin rotation measurements and specific heat experiments.[41–43] Our result is similar to that of the Chevrel phase superconductor $TlMo_6Se_{7.5}$,[44] in which NMR experiments also revealed a large gap, yet with no coherence peak due to the strong phonon damping that suppressed the coherence peak below T_c.[45]

4. Conclusion

We have grown single crystals of $(Sr_{1-x}Ca_x)_3Ir_4Sn_{13}$ ($x =$ 0, 0.5, 1) and $Ca_3Rh_4Sn_{13}$, and performed electrical resistivity and ^{119}Sn NMR measurements. In the normal state, we found an anomaly at T^* above the structural phase transition temperature T_s in $(Sr_{1-x}Ca_x)_3Ir_4Sn_{13}$ ($x = 0$, 0.5, 1). The NMR line width increases below T^* and $1/T_1T$ and K begin to decrease, followed by more distinct changes at T_s. None of these anomalies was observed in $Ca_3Rh_4Sn_{13}$ that does not undergo a structural phase transition. Our detailed analysis of $(Sr_{1-x}Ca_x)_3Ir_4Sn_{13}$ suggests antiferromagnetic spin fluctuations developing below T^* and becoming more visual below $T \sim 20$ K as a possible cause. The increase of T_c from $Sr_3Ir_4Sn_{13}$ to $Ca_3Rh_4Sn_{13}$ can be partly ascribed to the increase of the electronic DOS, but the antiferromagnetic spin fluctuations may also make a contribution. Remarkably, the precursory electronic anomaly shares a similarity with a phenomenon under active investigation in the Fe-based high-T_c superconductors where a change in the electronic properties expected at T^* occurs already above T_s. Therefore, our work sheds light on other correlated electron systems in a broad context.

In the superconducting state of $Ca_3Ir_4Sn_{13}$, the spin susceptibility vanishes at low temperature, indicating a spin-singlet electron pairing. The spin-lattice relaxation rate decays exponentially with decreasing temperature as $\exp(-\Delta/k_BT)$, which indicates a fully opened energy gap. The large superconducting gap $2\Delta = 4.42k_BT_c$ accompanied by a lack of the coherence peak indicates that $Ca_3Ir_4Sn_{13}$ is a strong-coupling superconductor.

References

[1] Moncton D E, Axe J D and Disalvo F J 1977 *Phys. Rev. B* **16** 801
[2] Takada K, Sakurai H, Takayama-Muromachi E, Izumi F, Dilanian R A and Sasaki T 2003 *Nature* **422** 53
[3] Stewart G R 2011 *Rev. Mod. Phys.* **83** 1589
[4] Lee P A, Nagaosa N and Wen X G 2006 *Rev. Mod. Phys.* **78** 17
[5] Mathur N D, Grosche F M, Julian S R, Walker I R, Freye D M, Haselwimmer R K W and Lonzarich G G 1998 *Nature* **394** 39
[6] Oka T, Li Z, Kawasaki S, Chen G F, Wang N L and Zheng G Q 2012 *Phys. Rev. Lett.* **108** 047001
[7] Zhou R, Li Z, Yang J, Sun D L, Lin C T and Zheng G Q 2013 *Nat. Commun.* **4** 2265
[8] Yang J, Zhou R, Wei, L L, Yang H X, Li J Q, Zhao Z X and Zheng G Q 2015 *Chin. Phys. Lett.* **32** 107401
[9] Kuo H H, Chu J H, Palmstrom J C, Kivelson S A and Fisher I R 2016 *Science* **352** 958
[10] Lederer S, Schattner Y, Berg E and Kivelson S A 2017 *Proc. Natl. Acad. Sci. USA* **114** 4905

[11] Remeika J P, Espinosa G P, Cooper A S, Barz H, Rowell J M, McWhan D B, Vandenberg J M, Moncton D E, Fisk Z, Woolf L D, Hamaker H C, Maple M B, Shirane G and Thomlinson W 1980 *Solid State Commun.* **34** 923

[12] Kase N, Hayamizu H and Akimitsu J 2011 *Phys. Rev. B* **83** 184509

[13] Espinosa G P 1980 *Mater. Res. Bull.* **15** 791

[14] Espinosa G P, Cooper A S and Barz H 1982 *Mater. Res. Bull.* **17** 963

[15] Yang J H, Chen B, Michioka C and Yoshimura K 2010 *J. Phys. Soc. Jpn.* **79** 113705

[16] Zhou S Y, Zhang H, Hong X C, Pan B Y, Qiu X, Dong W N, Li X L and Li S Y 2012 *Phys. Rev. B* **86** 064504

[17] Wang K F and Petrovic C 2012 *Phys. Rev. B* **86** 024522

[18] Klintberg L E, Goh S K, Alireza P L, Saines P J, Tompsett D A, Logg P W, Yang J H, Chen B, Yoshimura K and Grosche F M 2012 *Phys. Rev. Lett.* **109** 237008

[19] Goh S K, Tompsett D A, Saines P J, Chang H C, Matsumoto T, Imai M, Yoshimura K and Grosche F M 2015 *Phys. Rev. Lett.* **114** 097002

[20] Yu W C, Cheung Y W, Saines P J, Imai M, Matsumoto T, Michioka C, Yoshimura K and Goh S K 2015 *Phys. Rev. Lett.* **115** 207003

[21] Mazzone D G, Gerber S, Gavilano J L, Sibille R, Medarde M, Delley B, Ramakrishnan M, Neugebauer M, Regnault L P, Chernyshov D, Piovano A, Fernandez-Diaz T M, Keller L, Cervellino A, Pomjakushina E, Conder K and Kenzelmann M 2015 *Phys. Rev. B* **92** 024101

[22] Lue C S, Kuo C N, Tseng C W, Wu K K, Liang Y H, Du C H and Kuo Y K 2016 *Phys. Rev. B* **93** 245119

[23] Fang A F, Wang X B, Zheng P and Wang N L 2014 *Phys. Rev. B* **90** 035115

[24] Kuo C N, Liu H F, Lue C S, Wang L M, Chen C C and Kuo Y K 2014 *Phys. Rev. B* **89** 094520

[25] Chen B, Yang J, Guo Y and Yoshimura K 2015 *Euro. Phys. Lett.* **111** 17005

[26] Tompsett D A 2014 *Phys. Rev. B* **89** 075117

[27] Chu J H, Analytis J G, De Greve K, McMahon P L, Islam Z, Yamamoto Y and Fisher I R 2010 *Science* **329** 824

[28] Kasahara S, Shi H J, Hashimoto K, Tonegawa S, Mizukami Y, Shibauchi T, Sugimoto K, Fukuda T ,Terashima T, Nevidomskyy A H and Matsuda Y 2012 *Nature* **486** 382

[29] Zhou R, Xing L Y, Wang X C, Jin C Q and Zheng G Q 2016 *Phys. Rev. B* **93** 060502(R)

[30] Timusk T and Statt B 1999 *Rep. Prog. Phys.* **62** 61

[31] Kawasaki S, Tani Y, Mabuchi T, Kudo K, Nishikubo Y, Mitsuoka D, Nohara M and Zheng G Q 2015 *Phys. Rev. B* **91** 060510(R)

[32] Li Z, Jiao W H, Cao G H and Zheng G Q 2016 *Phys. Rev. B* **94** 174511

[33] Dahm T and Ueda K 2007 *Phys. Rev. Lett.* **99** 187003

[34] Nakai Y, Ishida K, Sugawara H, Kikuchi D and Sato H 2008 *Phys. Rev. B* **77** 041101(R)

[35] Toda M, Sugawara H, Magishi K, Saito T, Koyama K, Aoki Y and Sato H 2008 *J. Phys. Soc. Jpn.* **77** 124702

[36] Hu Y J, Cheung Y W, Yu W C, Imai M, Kanagawa H, Murakawa J, Yushimura K and Goh S K 2017 *Phys. Rev. B* **95** 155142

[37] Maeda S, Matano K, Yatagai R, Oguchi T and Zheng G Q 2015 *Phys. Rev. B* **91** 174516

[38] Zheng G Q, Ozaki H, Kitaoka Y, Kuhns P, Reyes A P and Moulton W G 2002 *Phys. Rev. Lett.* **88** 077003

[39] Kotegawa H, Yogi M, Imamura Y, Kawasaki Y, Zheng G Q, Kitaoka Y, Ohsaki S, Sugawara H, Aoki Y and Sato H 2003 *Phys. Rev. Lett.* **90** 027001

[40] Sarkar R, Brueckner F, Guenther M, Wang K F, Petrovic C, Biswas P K, Luetkens H, Morenzoni E, Amato A and Klauss H H 2015 *Physica B* **479** 51

[41] Gerber S, Gavilano J L, Medarde M, Pomjakushin V, Baines C, Pomjakushina E, Conder K and Kenzelmann M 2013 *Phys. Rev. B* **88** 104505

[42] Biswas P K, Guguchia Z, Khasanov R, Chinotti M, Li L, Wang K F, Petrovic C and Morenzoni E 2015 *Phys. Rev. B* **92** 195122

[43] Hou J, Wong C H, Lortz R, Sibille R and Kenzelmann M 2016 *Phys. Rev. B* **93** 134505

[44] Kitaoka Y, Ohsugi S, Asayama K and Ohtani T 1992 *Physica C* **192** 272

[45] Allen P B and Rainer D 1991 *Nature* **349** 396